www.sciencemag.org/content/346/6214/1227/suppl/DC1

Supplementary Materials for

Multidecadal warming of Antarctic waters

Sunke Schmidtko,* Karen J. Heywood, Andrew F. Thompson, Shigeru Aoki

*Corresponding author. E-mail: sschmidtko@geomar.de

Published 5 December 2014, *Science* **346**, 1227 (2014)
DOI: 10.1126/science.1256117

This PDF file includes:

Materials and Methods:

We combined conductivity, temperature, depth (CTD) profiles from seven publicly available databases (Tab. S1) and mapped the properties of ASBW, WW, CDW and their associated trends since 1975. Due to limited data (Fig. S1) in this remote area, not all regions resolve the same period (Fig S2). Duplicates were avoided by checking for repeat profiles within 5 km and 25 h, allowing for rounding errors in latitude, longitude and time. In the rare case that 2 or more CTD casts were made within these temporal and spatial scales, we treat them as duplicates and only use one. When duplicate profiles were identified, the profile with the best vertical resolution was used. Profiles with a vertical resolution coarser than 20m were rejected; this filter is not applied to float data.

ASBW is defined using the deepest measurement in profiles within 30m of the bottom, or, in the absence of CTD altimeter data, within 150m of the ETOPO-1 bathymetry (*29*). This depth provides an estimate of uncertainty for the mapped bathymetry, since 5% of profiles exceed the bathymetry by up to 150 m. The cores of WW and CDW are defined by the conservative temperature (Θ) minimum below 40 m and the Θ maximum below the minimum, respectively.

ASBW data are mapped onto a 0.25°x0.125° grid for bathymetry shallower than 1500 m, while CDW and WW are mapped on a 0.5°x0.5° grid for bathymetry deeper than 1500 m. We apply the ETOPO-1 bathymetry for our analysis (*29*). For each grid point in our maps, the horizontal distance to data positions is derived by a Fast Marching algorithm (*13*). The algorithm uses a 300 m scaling in bathymetry difference and a minimum propagation of 0.1 on a 18x18 km grid for the speed map. This algorithm determines the along-path distance between the grid point to be mapped and data locations, including distance penalties for moving across bathymetry with different depths. Over the continental slope, the mapping is predominantly along bathymetric contours. Over flat bathymetry, the algorithm would result in a circular region of influence,

however over rough, highly-variable terrain, the distances may be significantly longer in some directions (Fig. S7, S8). Only data at locations that can be reached with this marching algorithm are used.

Data are normally-weighted using an along-pathway horizontal scaling of 400 km. A vertical scaling of 200 dbar is applied for ASBW, but no vertical weighting is applied for WW and CDW. The vertical weighting for ASBW allows us to better differentiate ASBW properties and trends in troughs, canyons and other small-scale features on the shelf, which are not resolved in the ETOPO-1 data set (*29*). As a final step before mapping, an interquartile range (IQR) filter is applied to all parameters. Values more than twice the IQR below the first quartile or more than twice the IQR above the third quartile are rejected. We then apply a weighted least-squares linear model (*30*) (LOESS) at each grid point to all data with positive weights larger than 10^{-3}. The model removes linear fits for longitude and latitude in the fast marching-derived coordinate system (*13*) as well as in depth for the shelf mapping. This LOESS model is used to determine the mean state and temporal trend of water mass properties. The spatial trend removal in the Fast Marching derived coordinate system accounts for across and along slope gradients for any resolved bathymetry (Fig. S7).

Statistically significant are trends that are larger than twice the 'estimated standard error' of the least squares solution. The 5-yr median properties of ASBW (Fig. 1E, F, S3, S5) are computed from the difference between raw data and the mapped properties, offset by the median mapped temperature and salinity.

Table S1. Data sources of used CTD data

Name	Website	Date accessed.	Comment
Argo floats	http://argo.ucsd.edu	05/2012	All data flagged good
World Ocean Database	http://www.nodc.noaa.gov/OC5/WOD09/pr_wod09.html	05/2013	All CTD data flagged good or probably good
Hydrobase 3	http://www.whoi.edu/science/PO/hydrobase/	06/2013	All CTD data used
Cliver and Carbon Hydrographic Database	http://cchdo.ucsd.edu/	01/2013	All CTD data available in netCDF format
Southern Ocean Database	http://woceatlas.tamu.edu/Sites/html/atlas/SOA_DATABASE.html	05/2013	All CTD data used
British Oceanographic Database	https://www.bodc.ac.uk/	06/2013	All data CTD flagged good
Pangaea database	http://www.pangaea.de/	05/2013	All Polarstern CTD data publically available

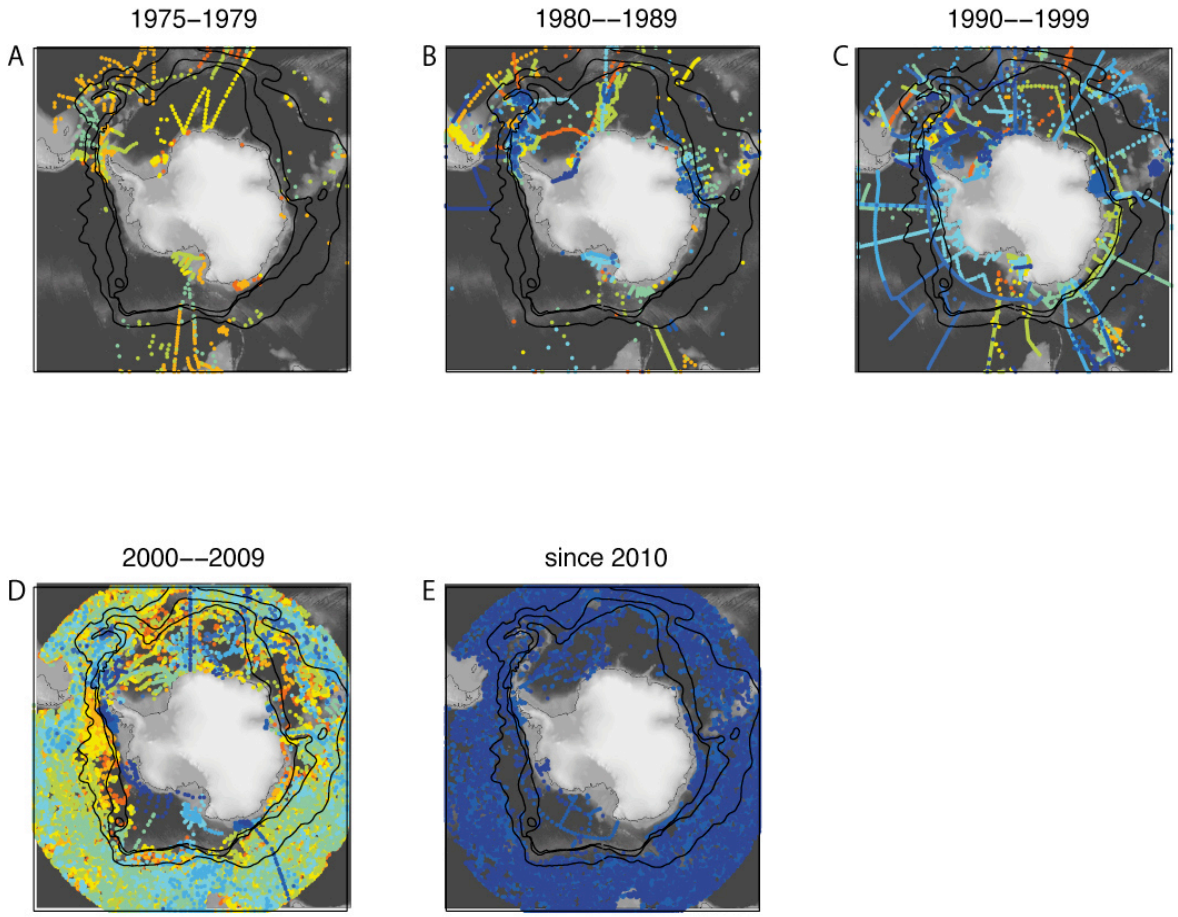

Fig. S1. Data coverage for each decade. A, Profile location from the period 1975–1979 and position of Antarctic Circumpolar Current fronts. B-E, similar to (A) for the successive decades. The individual years for each period are color-coded from blue (year 0) to red (year 9). Fronts (*28*) related to the ACC are shown as black lines.

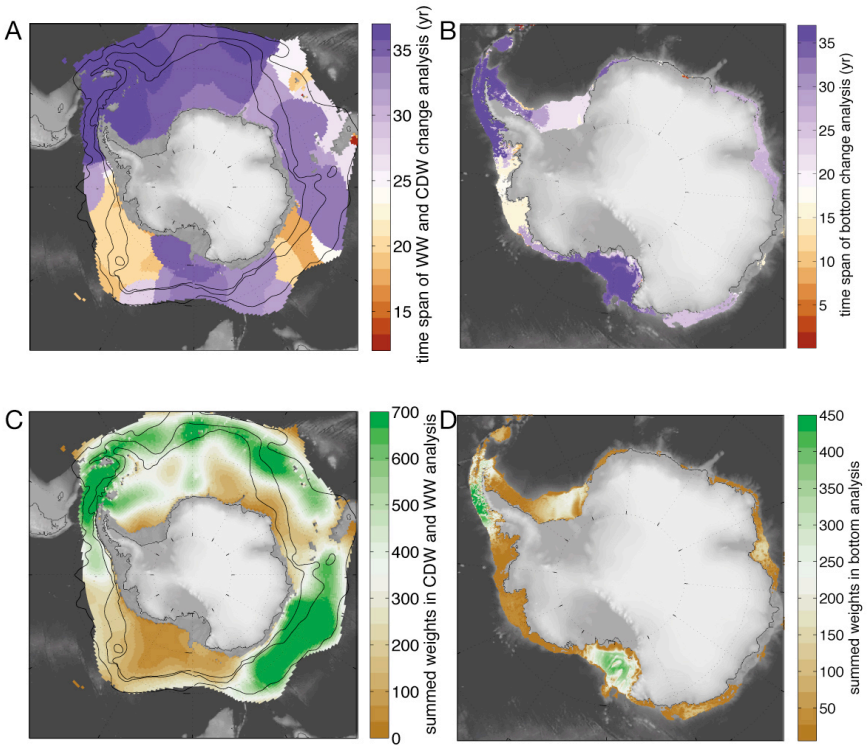

Fig. S2. Data density. A, Time span of linear trend computation for CDW and WW. B, similar to (A) for the bottom water analysis on the shelf. C, sum of weights used in Gaussian LOESS mapping at each grid point. D, similar to (C) for the on shelf bottom water analysis. Fronts (*28*) related to the ACC are shown as black lines.

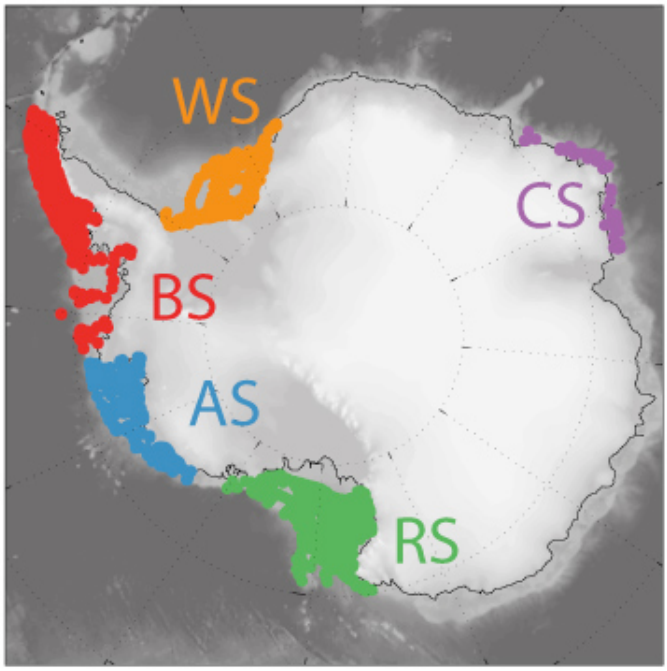

Fig. S3. Area extent and location of data used for the 5-yr bin average in Fig. 1E,F. Profile location from the period 1975–2012 for selected areas around Antarctica.

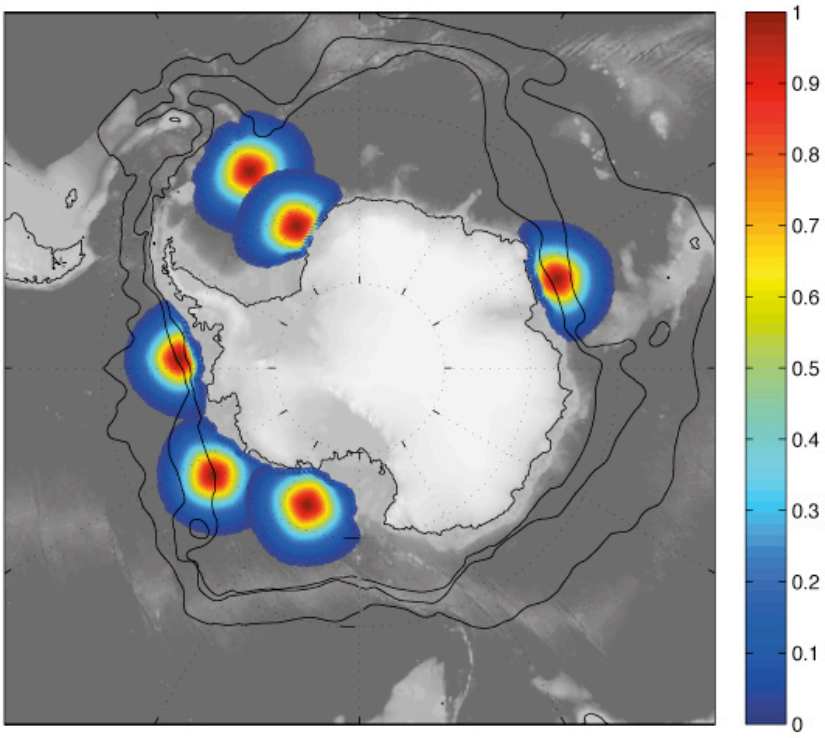

Fig. S4. Locations and distance weighting. Weights for LOESS mapping for the 6 regions used in Fig. 2G. The bathymetry-following mapping scheme does not include data from the shelf and reduces the weights rapidly under changing bathymetry. The center locations are assigned a weight of one with a Gaussian decay and a half folding scale of 400km. Fronts (*28*) related to the ACC are shown as black lines.

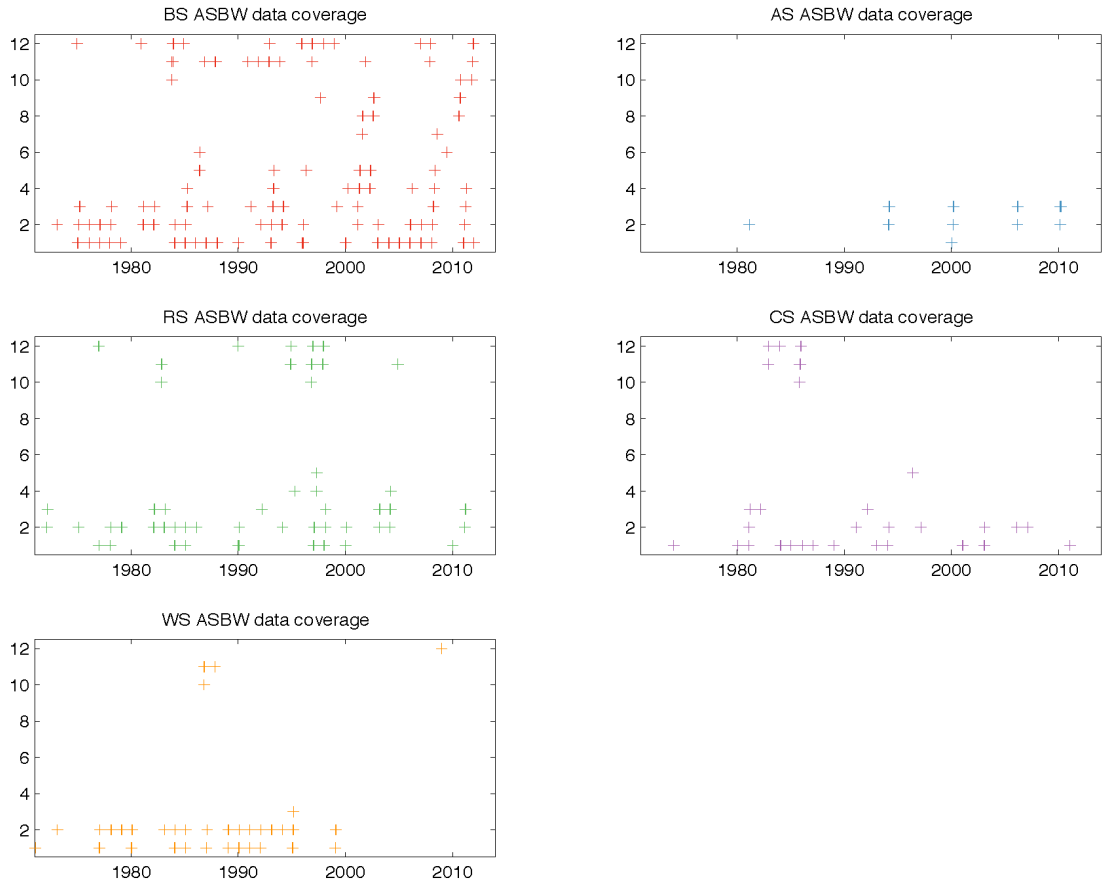

Fig. S5. Temporal data distribution as used for selected ASBW regions. Profile year and month of data for the 5 selected regions as shown in Fig. S5. These data are used for the 5-yr binned averages and inter quartile ranges in Fig. 1E,F.

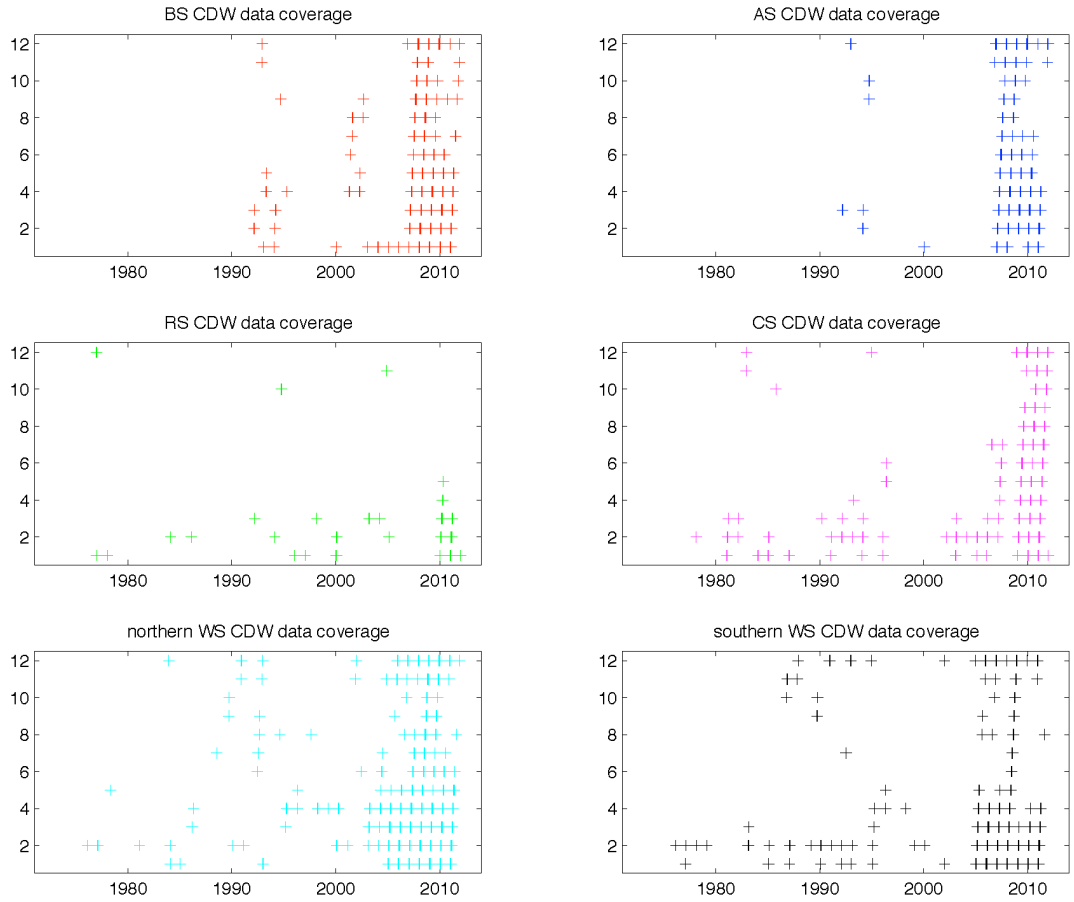

Fig. S6. Temporal data distribution as used for selected CDW regions. Profile year and month of data for the 6 selected regions as shown in Fig. S6. These data are used for the 5-yr binned averages and inter quartile ranges in Fig. 2G.

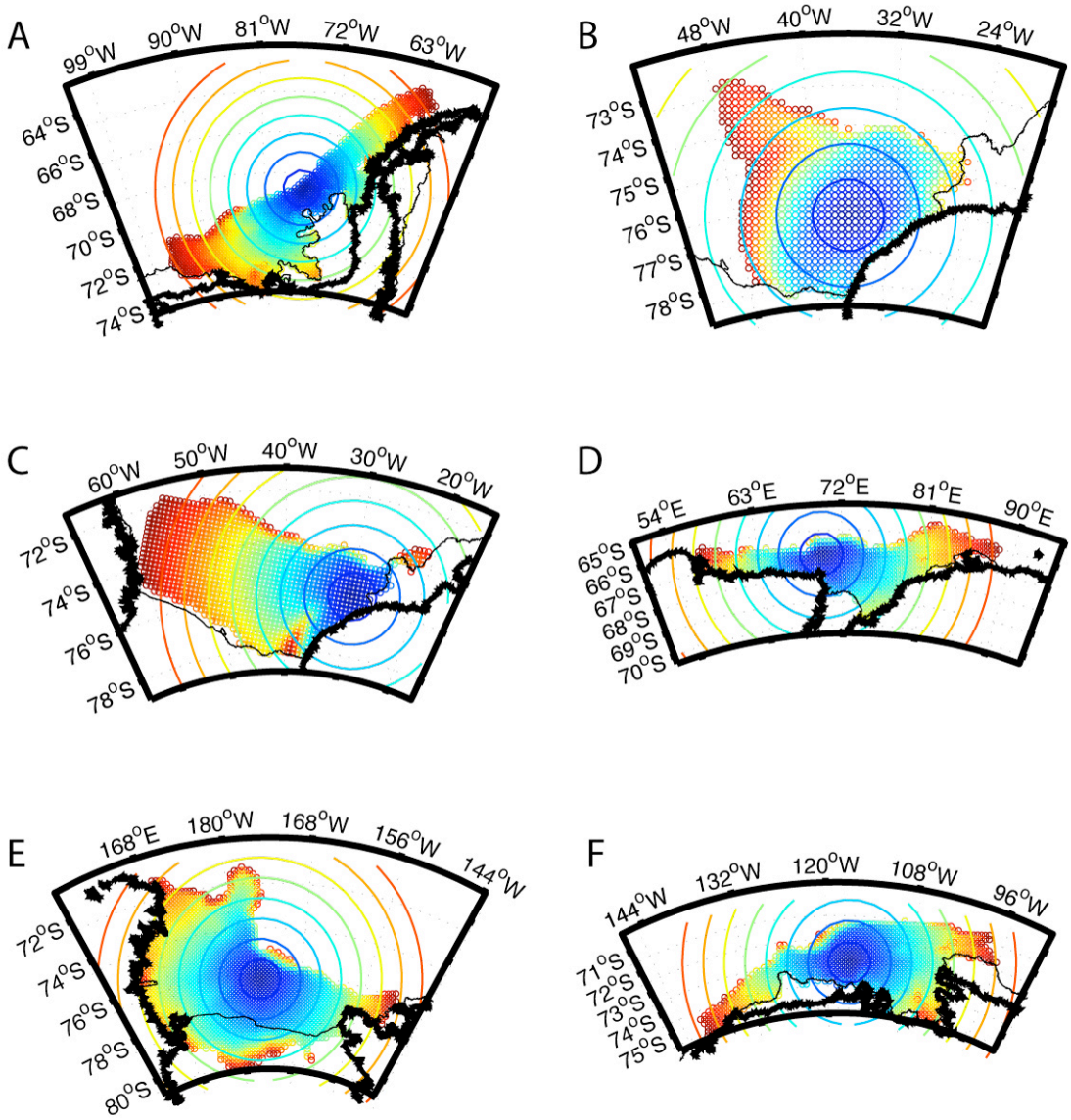

Fig. S7. Fast marching distances on the Antarctic shelf for selected shelf locations. The large circles indicate a circular influence region with contour spacing of 100km. Small circles indicate the locations reached by the fast marching algorithm and the assigned distance, using the same color coding as the large circles. The mapped regions are (A) the west Antarctic Peninsula, (B, C) the south western Weddell Sea for different locations, (D) the Cosmonaut Sea, (E) the Ross Sea and (F) the Amundsen Sea.

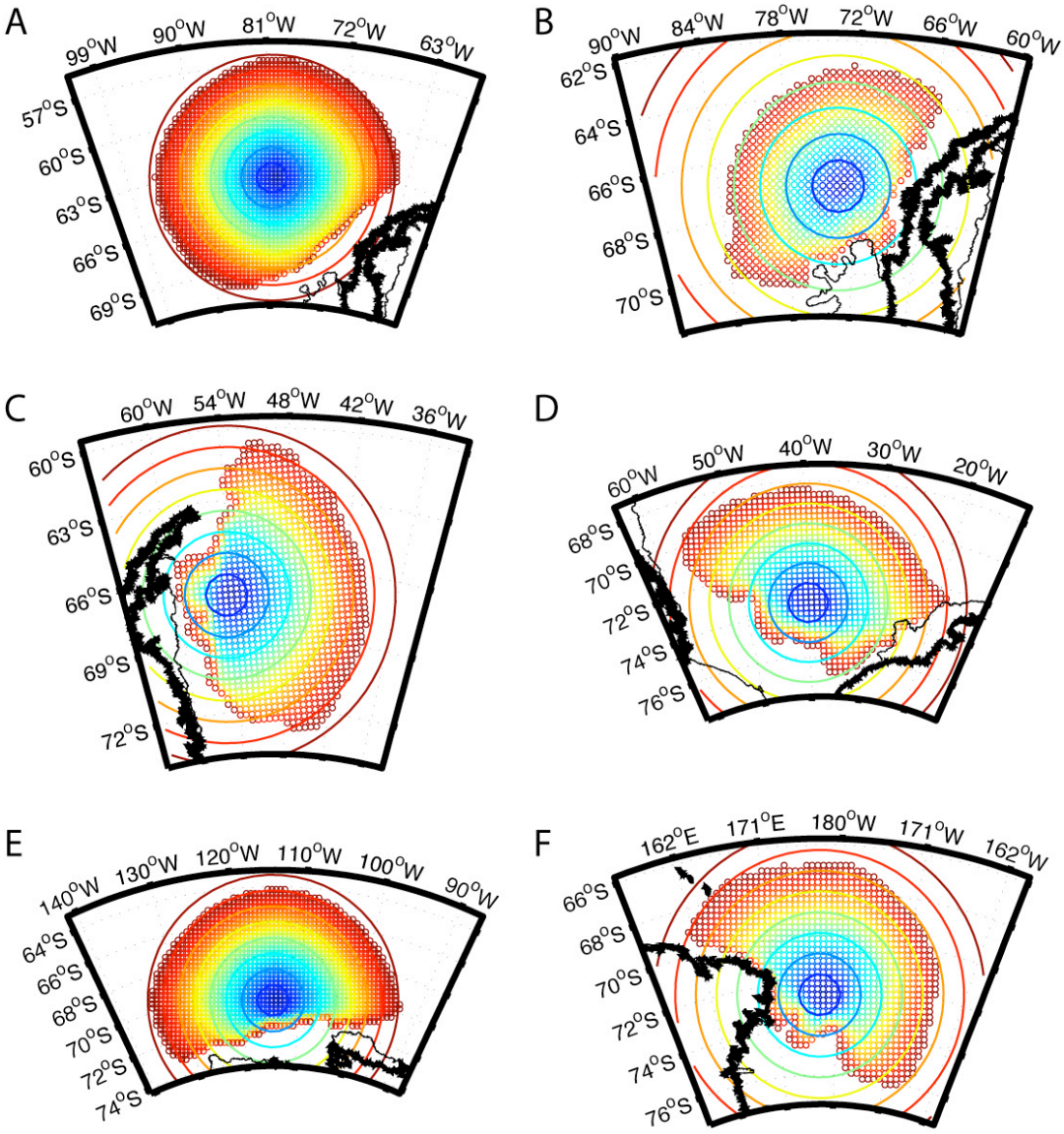

Fig. S8. Fast marching derived distances around Antarctic for selected continental slope locations. The large circles indicate a circular influence region with contour spacing of 100km. Small circles indicate the locations reached by the fast marching algorithm and the assigned distance, using the same color coding as the large circles. The mapped CDW regions are (A,B) Bellinghausen Sea, (C,D) Weddell Sea, (E) Amundsen Sea and (F) Ross Sea.

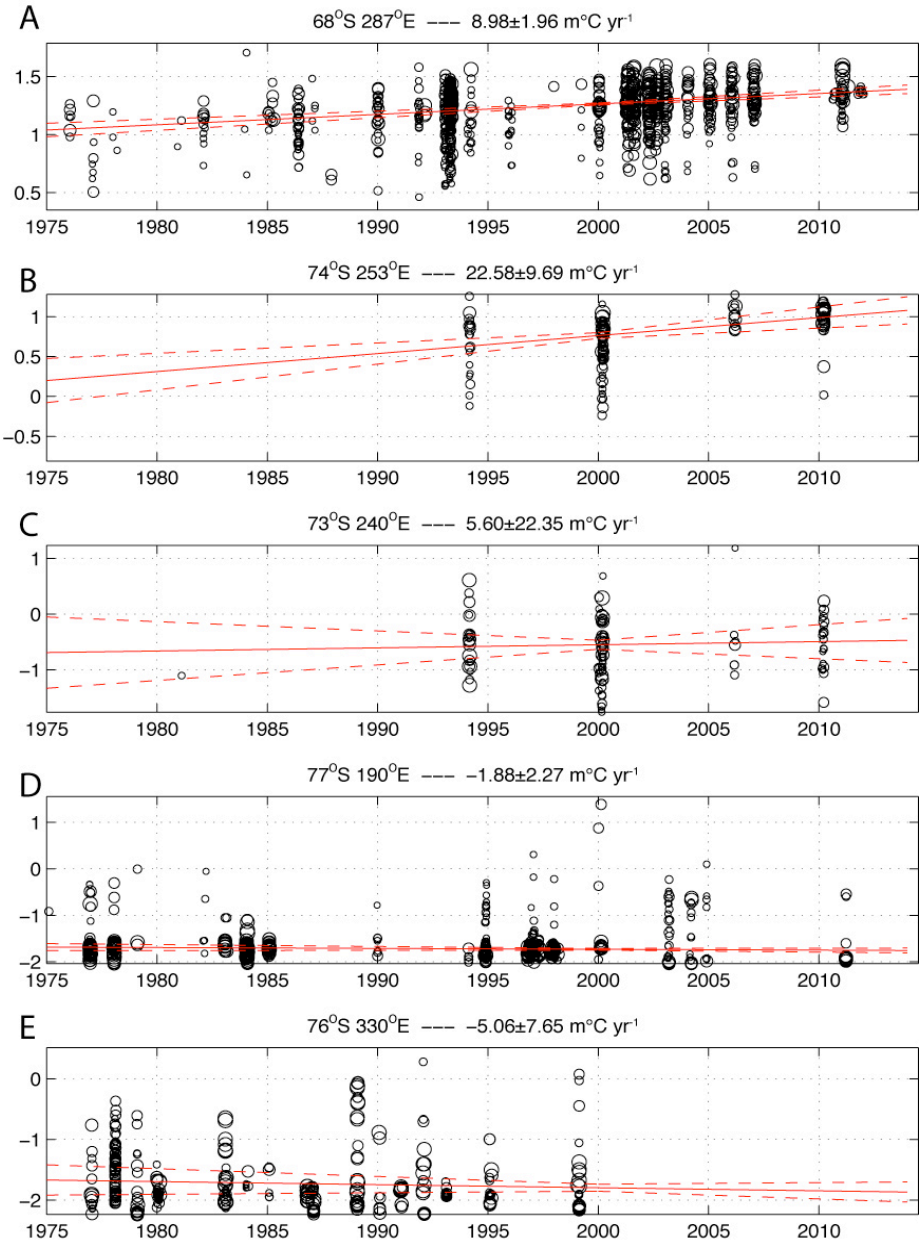

Fig. S9. Raw data distribution and trends for selected locations. Red lines indicate the trend (solid line) as well as uncertainty in the trend (dashed line). Uncertainties are given as twice the standard error. The trend is regarded as significant if it is larger than twice the standard error of the trend. Each circle is a data point, the size of the circle indicates the weight for the final mapping, using horizontal and vertical scaling (Fig. S7, methods). The regions are (A) Bellinghausen Sea, (B) Amundsen Sea – significant trend, (C) Amundsen Sea – non significant trend, (D) Ross Sea and (E) Weddell Sea.

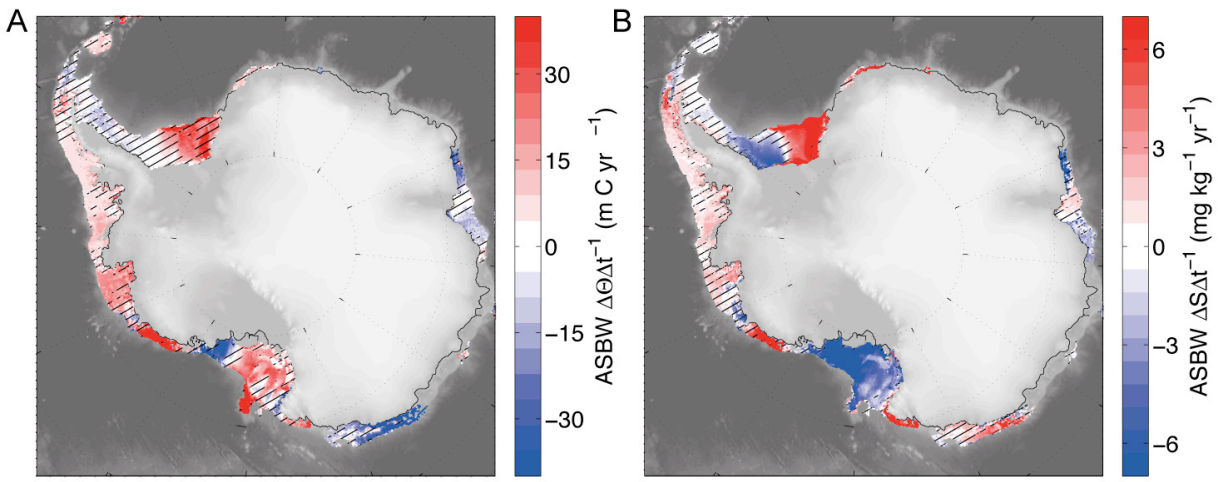

Fig. S10. Similar to Fig. 1C, D but for trends of ASBW using only data since 1990. Some areas, like the Weddell Sea shelf have very poor data coverage in recent decades, and trends shown might not represent the longer term change during this period, see Fig S1, S2, S5 for data coverage. Fig. 1C, D represent the ASBW long-term changes.

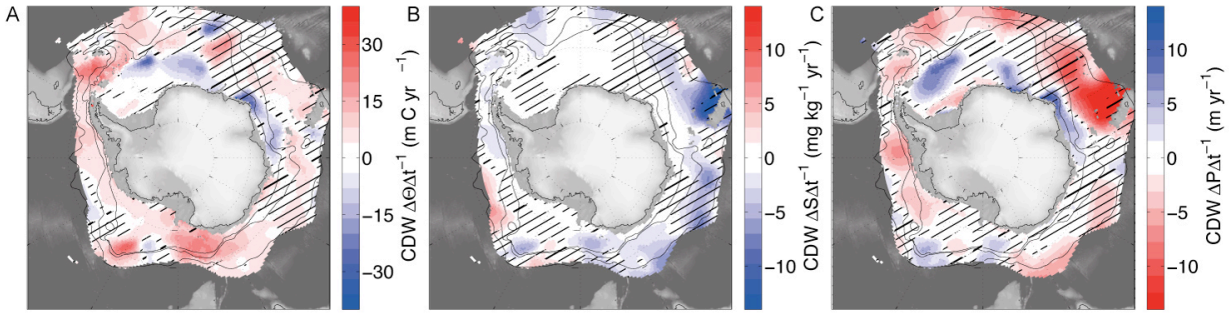

Fig. S11. Similar to Fig. 2 D–F but for trends of CDW using only data since 1990. Although the basic patterns are similar to those with data since 1975 (Fig. 2D–F) treat trends over this shorter time period with caution, see Figs. S1, S2, S6 for data coverage. Fig. 2D–F represent the CDW long-term changes. Fronts (*28*) related to the ACC are shown as black lines.

References

1. A. Shepherd, E. R. Ivins, G. A, V. R. Barletta, M. J. Bentley, S. Bettadpur, K. H. Briggs, D. H. Bromwich, R. Forsberg, N. Galin, M. Horwath, S. Jacobs, I. Joughin, M. A. King, J. T. Lenaerts, J. Li, S. R. Ligtenberg, A. Luckman, S. B. Luthcke, M. McMillan, R. Meister, G. Milne, J. Mouginot, A. Muir, J. P. Nicolas, J. Paden, A. J. Payne, H. Pritchard, E. Rignot, H. Rott, L. S. Sørensen, T. A. Scambos, B. Scheuchl, E. J. Schrama, B. Smith, A. V. Sundal, J. H. van Angelen, W. J. van de Berg, M. R. van den Broeke, D. G. Vaughan, I. Velicogna, J. Wahr, P. L. Whitehouse, D. J. Wingham, D. Yi, D. Young, H. J. Zwally, A reconciled estimate of ice-sheet mass balance. *Science* **338**, 1183–1189 (2012). Medline doi:10.1126/science.1228102

2. H. De Angelis, P. Skvarca, Glacier surge after ice shelf collapse. *Science* **299**, 1560–1562 (2003). Medline doi:10.1126/science.1077987

3. I. Joughin, B. E. Smith, B. Medley, Marine ice sheet collapse potentially under way for the Thwaites Glacier Basin, West Antarctica. *Science* **344**, 735–738 (2014). Medline doi:10.1126/science.1249055

4. E. Rignot, S. S. Jacobs, Rapid bottom melting widespread near Antarctic Ice Sheet grounding lines. *Science* **296**, 2020–2023 (2002). Medline doi:10.1126/science.1070942

5. H. D. Pritchard, S. R. Ligtenberg, H. A. Fricker, D. G. Vaughan, M. R. van den Broeke, L. Padman, Antarctic ice-sheet loss driven by basal melting of ice shelves. *Nature* **484**, 502–505 (2012). Medline doi:10.1038/nature10968

6. A. A. Petty, D. L. Feltham, P. R. Holland, Impact of atmospheric forcing on Antarctic continental shelf water masses. *J. Phys. Oceanogr.* **43**, 920–940 (2013). doi:10.1175/JPO-D-12-0172.1

7. P. Spence, S. M. Griffies, M. H. England, A. M. Hogg, O. A. Saenko, N. C. Jourdain, Rapid subsurface warming and circulation changes of Antarctic coastal waters by poleward shifting winds. *Geophys. Res. Lett.* **41**, 2014GL060613 (2014). doi:10.1002/2014GL060613

8. S. S. Jacobs, C. F. Giulivi, Large multidecadal salinity trends near the Pacific-Antarctic continental margin. *J. Clim.* **23**, 4508–4524 (2010). doi:10.1175/2010JCLI3284.1

9. H. H. Hellmer, O. Huhn, D. Gomis, R. Timmermann, On the freshening of the northwestern Weddell Sea continental shelf. *Ocean Sci.* **7**, 305–316 (2011). doi:10.5194/os-7-305-2011

10. S. T. Gille, Decadal-scale temperature trends in the Southern Hemisphere ocean. *J. Clim.* **21**, 4749–4765 (2008). doi:10.1175/2008JCLI2131.1

11. S. G. Purkey, G. C. Johnson, Warming of global abyssal and Deep Southern Ocean waters between the 1990s and 2000s: Contributions to global heat and sea level rise budgets. *J. Clim.* **23**, 6336–6351 (2010). doi:10.1175/2010JCLI3682.1

12. M. Azaneu, R. Kerr, M. M. Mata, C. A. E. Garcia, Trends in the deep Southern Ocean (1958-2010): Implications for Antarctic Bottom Water properties and volume export. *J. Geophys. Res. Oceans* **118**, 4213–4227 (2013). doi:10.1002/jgrc.20303

13. S. Schmidtko, G. C. Johnson, J. M. Lyman, MIMOC: A global monthly isopycnal upperocean climatology with mixed layers. *J. Geophys. Res. Oceans* **118**, 1658–1672 (2013). doi:10.1002/jgrc.20122

14. S. G. Purkey, G. C. Johnson, Antarctic Bottom Water warming and freshening: Contributions to sea level rise, ocean freshwater budgets, and global heat gain. *J. Clim.* **26**, 6105–6122 (2013). doi:10.1175/JCLI-D-12-00834.1

15. P. R. Holland, R. Kwok, Wind-driven trends in Antarctic sea-ice drift. *Nat. Geosci.* **5**, 872–875 (2012). doi:10.1038/ngeo1627

16. R. Bintanja, G. J. van Oldenborgh, S. S. Drijfhout, B. Wouters, C. A. Katsman, Important role for ocean warming and increased ice-shelf melt in Antarctic sea-ice expansion. *Nat. Geosci.* **6**, 376–379 (2013). doi:10.1038/ngeo1767

17. A. L. Stewart, A. F. Thompson, Sensitivity of the ocean's deep overturning circulation to easterly Antarctic winds. *Geophys. Res. Lett.* **39**, L18604 (2012). doi:10.1029/2012GL053099

18. P. Dutrieux, J. De Rydt, A. Jenkins, P. R. Holland, H. K. Ha, S. H. Lee, E. J. Steig, Q. Ding, E. P. Abrahamsen, M. Schröder, Strong sensitivity of Pine Island ice-shelf melting to climatic variability. *Science* **343**, 174–178 (2014). Medline doi:10.1126/science.1244341

19. H. H. Hellmer, F. Kauker, R. Timmermann, J. Determann, J. Rae, Twenty-first-century warming of a large Antarctic ice-shelf cavity by a redirected coastal current. *Nature* **485**, 225–228 (2012). Medline doi:10.1038/nature11064

20. M. S. Dinniman, J. M. Klinck, E. E. Hofmann, Sensitivity of Circumpolar Deep Water transport and ice shelf basal melt along the west Antarctic Peninsula to changes in the winds. *J. Clim.* **25**, 4799–4816 (2012). doi:10.1175/JCLI-D-11-00307.1

21. C. Heuzé, K. J. Heywood, D. P. Stevens, J. K. Ridley, Southern Ocean bottom water characteristics in CMIP5 models. *Geophys. Res. Lett.* **40**, 1409–1414 (2013). doi:10.1002/grl.50287

22. S. R. Rintoul, Rapid freshening of Antarctic Bottom Water formed in the Indian and Pacific oceans. *Geophys. Res. Lett.* **34**, L06606 (2007). doi:10.1029/2006GL028550

23. W. Zenk, E. Morozov, Decadal warming of the coldest Antarctic Bottom Water flow through the Vema Channel. *Geophys. Res. Lett.* **34**, L14607 (2007). doi:10.1029/2007GL030340

24. A. Atkinson, V. Siegel, E. Pakhomov, P. Rothery, Long-term decline in krill stock and increase in salps within the Southern Ocean. *Nature* **432**, 100–103 (2004). Medline doi:10.1038/nature02996

25. A. Atkinson, V. Siegel, E. A. Pakhomov, P. Rothery, V. Loeb, R. M. Ross, L. B. Quetin, K. Schmidt, P. Fretwell, E. J. Murphy, G. A. Tarling, A. H. Fleming, Oceanic circumpolar habitats of Antarctic krill. *Mar. Ecol. Prog. Ser.* **362**, 1–23 (2008). doi:10.3354/meps07498

26. L. J. Grange, C. R. Smith, Megafaunal communities in rapidly warming fjords along the West Antarctic Peninsula: Hotspots of abundance and beta diversity. *PLOS ONE* **8**, e77917 (2013). Medline doi:10.1371/journal.pone.0077917

27. E. Rignot, J. Mouginot, M. Morlighem, H. Seroussi, B. Scheuchl, Widespread, rapid grounding line retreat of Pine Island, Thwaites, Smith, and Kohler glaciers, West Antarctica, from 1992 to 2011. *Geophys. Res. Lett.* **41**, 3502–3509 (2014). doi:10.1002/2014GL060140

28. A. H. Orsi, T. Whitworth III, W. D. Nowlin Jr., On the meridional extent and fronts of the Antarctic Circumpolar Current. *Deep Sea Res. I* **42**, 641–673 (1995). doi:10.1016/0967-0637(95)00021-W

29. C. Amante, B. W. Eakins, *ETOPO1 1 Arc-Minute Global Relief Model: Procedures, Data Sources and Analysis* (National Geophysical Data Center, Boulder, CO, 2009); www.ngdc.noaa.gov/mgg/global/relief/ETOPO1/docs/ETOPO1.pdf.

30. W. S. Cleveland, S. J. Devlin, Locally weighted regression: An approach to regression analysis by local fitting. *J. Am. Stat. Assoc.* **83**, 596–610 (1988). doi:10.1080/01621459.1988.10478639